ORIGINAL PAPER

Size variant spherical gold nanoparticles for in situ detection of trace contaminants by surface enhanced Raman spectroscopy

Md. Shaha Alam[1] · Nazmul Islam Tanvir[1,2] · Mohammad Moniruzzaman[1] · Md Aftab Ali Shaikh[3,4] · Syed Farid Uddin Farhad[1,2]

Abstract

Spherical gold nanoparticles (AuNPs) of different sizes have been synthesized for the in situ detection of trace contaminants by Surface Enhanced Raman Spectroscopy (SERS) with Rhodamine 6G (R6G) as a probe molecule. TEM analyses revealed that most of the AuNPs are uniform in size and spherical in shape with an average dia. of $\sim 12 \pm 1$ nm and $\sim 25 \pm 3$ nm for solution pH 10.0 (GNP-10) and pH 6.0 (GNP-6), respectively. HR TEM lattice fringe analyses exhibit a consistent expansion of d-spacing for smaller GNP-10 compared to those of larger GNP-6 nanoparticles elucidated from both Au(111) and Au(200) planes. The SERS enhancement factor was calculated to be $\sim$20-fold larger for GNP-6 compared to that of GNP-10 while ~ 5 μL of AuNPs solution added in situ atop the 0.2×10^{-3} M R6G droplet (size ~ 4 mm) for Raman spectra recorded for ~ 5 s. Following this liquid phase SERS protocol, the detection limit as low as 10^{-11} M of R6G was successfully demonstrated.

Introduction

There has been tremendous attention in detecting trace-level chemical contaminants such as pesticides, adulterants, antibiotics, illegal drugs, and hazardous dyes that are harmful to humans and the environment. One of the major limitations in effectively managing chemical contaminants is the absence of rapid, precise, and efficient methods to detect, identify, and quantify toxic substances in complex samples. Numerous molecular methods have been developed based on optical, electrochemical, electronic, or gravimetric procedures to quantify these contaminants such as high-performance liquid chromatography (HPLC), immunological assays, surface-enhanced Raman spectroscopy (SERS), polymerase chain reaction (PCR) and liquid chromatography–mass spectrometry (LC–MS) [1, 2]. Among them, SERS is one of the best candidates for ultratrace and single-molecule level detection through molecular fingerprint specificity [3, 4]. SERS utilizes the surface plasmon resonance (SPR) features of nanostructures to enormously enhance the Raman scattering signals of samples understudy. Therefore, the development of facile and cost-effective SERS protocols holds great promise for advancing this technology across a spectrum of applications, mitigating the need for extensive sample preparation, which will pave the way for practical implementation in diverse fields ranging from pharmaceuticals to biomedical diagnostics, materials sciences to environmental monitoring [5–8]. In SERS amplification, two main mechanisms such as the chemical mechanism (CM) and the electromagnetic mechanism (EM) are involved. The CM arises from the localized charge transfer that originates in the nanomaterials whereas the EM mechanism is due to the enhanced local electric field that causes a significant increase in the Raman scattering. As a result, for SERS substrates metallic nanoparticles (for example, Ag, Cu, and Au) have drawn a lot of interest [9]. Among them, Gold (Au) nanoparticles (NPs) have received the most attention due to their biocompatible, optical, electric, and chemical characteristics [10]. Moreover, the efficiency of surface-enhanced Raman scattering

Md. Shaha Alam and Nazmul Islam Tanvir have made equal contribution to this work.

✉ Syed Farid Uddin Farhad
s.f.u.farhad@bcsir.gov.bd; sf1878@my.bristol.ac.uk

1 Central Analytical and Research Facilities (CARF), BCSIR, Dhaka 1205, Bangladesh

2 Energy Conversion and Storage Research Section, Industrial Physics Division, BCSIR Dhaka Laboratories, BCSIR, Dhaka 1205, Bangladesh

3 Bangladesh Council of Scientific and Industrial Research (BCSIR), Dhaka 1205, Bangladesh

4 Department of Chemistry, University of Dhaka, Dhaka 1000, Bangladesh

(SERS) substrates is greatly dominated by the size and shape of the AuNPs. The smaller AuNPs (< 60 nm) compared to larger ones can lead to a gigantic SERS enhancement due to their large surface-to-volume ratio [11, 12] as well as the combination of resonance matching of two or more nanostructures and enhanced surface adsorption of analytes on the nanostructures. To this end, tremendous efforts have been made to control the mean size, shape, and surface morphology to produce optimum-size AuNPs [13, 14]. In 1998, Emory et al. demonstrated size-dependent SERS enhancement in single metal nanoparticles and later in 2006, Plech's group revisited the Turkevich method for gold nanoparticle synthesis [15, 16]. In our previous study, we demonstrated that spherical shapes AuNPs exhibit a better SERS enhancement than that of rod-shaped AuNPs [17] utilizing a 785 nm laser as a Raman excitation source. In this study, using spherical AuNPs of optimized size, we demonstrated a facile liquid phase SERS protocol for in situ detection of low-level contaminants present in pharmaceuticals, agriculture, and fruits and foodstuffs. In this direction, different sizes of spherical AuNPs were prepared to assess their utility to detect the lower detection (LoD) limit of Rhodamine 6G (R6G), as a *proof-of-concept*. The suggested method in this study is easily adaptable for quick identification of hazardous chemicals in the liquid phase because there is no need for extensive sample preparation/modification.

Materials and methods

Synthesis of gold nanoparticles

The chemicals used for AuNPs synthesis were chloroauric acid ($HAuCl_4$, Sigma-Aldrich), sodium citrate dihydrate ($Na_3C_6H_5O_7·2H_2O$, Sigma-Aldrich), hydrochloric acid (HCl, reagent grade, 37%, Sigma-Aldrich) and nitric acid (HNO_3, ACS reagent grade, 70%, Ricca Chemical). Rhodamine 6G (R6G, Sigma-Aldrich) was used as a probe molecule. The detailed synthesis procedure of AuNPs can be found in our previous study [17] and the Supplementary Information (SI) file. However, the molar ratio of chloroauric acid ($HAuCl_4$) and sodium citrate dihydrate (SCD); ($HAuCl_4$/SCD) was 2:1 and 1:2 respectively at pH ~ 6.0 and ~ 10.0. Hereafter, gold nanoparticles grown from lower and higher SCD molar concentrations are labeled as "GNP-6" and "GNP-10" respectively for convenience. The deionized (DI) water (~ 18.2 MΩ cm) was used to prepare all solutions.

Characterizations

Before instrumental characterization, the AuNPs solution was centrifuged at 10,000 rpm for 15 min. After centrifugation, the precipitated AuNPs were collected and dispersed in DI water. This procedure was repeated 5 times. Then the unreactive SCD-free AuNPs solution's electronic absorption spectra for the maximum surface plasmon resonance (SPR) wavelength (λ_{max}) were determined using a Shimadzu 2600 UV–Vis–NIR spectrometer. Zeta potential and particle diameter measurements were conducted using a Dynamic Light Scattering (DLS) instrument (Horiba SZ-100V2) with a minimum of three consecutive measurements to confirm its accuracy. The average diameter of nanoparticles was estimated from the peak maxima of DLS size distribution curves. For morphology/shape, size distribution, crystal structure, and chemical information of synthesized AuNPs were examined by a Transmission Electron Microscope (TEM) (Talos F200XG2, ThermoFisher SCIENTIFIC). TEM specimen preparation can be found in the SI file. The SERS spectra were recorded using a Raman spectrometer (Horiba MacroRam, USA) equipped with a 785 nm diode laser. We used the R6G (0.2×10^{-3} M) droplet of ~ 3 mm diameter on the pre-cleaned Stainless Steel (SS) substrate as a Raman probe. For the limit of detection (LoD) of R6G, the stock solution of R6G (0.2×10^{-3} M) was sequentially diluted in different concentrations from 0.1×10^{-3} ($= 10^{-4}$) to 10^{-11} M using DI water. Then ~ 5 μL GNP-6 and GNP-10 solutions are added atop the R6G droplet (diameter ~ 3 mm) separately and the SERS spectra are taken immediately with an acquisition time of ~ 5 s if not mentioned otherwise.

Results and discussion

UV–Vis–NIR absorption spectroscopy and particle sizing with Zeta potential

UV–Vis absorption spectroscopy is considered one of the foremost techniques for evaluating the optical nature of nanoparticles [18]. Figure 1a shows the absorbance of R6G (inset shows the chemical structure) with three peaks near 527 nm, 347 nm, and 248 nm with significantly dominant absorption at 527 nm called absorbance maxima (λ_{max}). The AuNPs can possess different SPR bands due to the excitation of electron clouds by the incident electromagnetic wave. The electron cloud can oscillate on the nanoparticle's surface by absorbing electromagnetic radiation with a certain amount of energy at their nanoscales. Due to their surface sensitivity, SPR is a useful tool for monitoring adsorption onto particle surfaces [19]. As can be seen from Fig. 1b, the SPR bands were shifted from a lower wavelength of 519 nm to a higher wavelength of 523 nm with the decrease of SCD molar concentration with respect to $HAuCl_4$ from $HAuCl_4$/SCD = 1:2 (GNP-10) to $HAuCl_4$/SCD = 2:1 (GNP-6). It can be inferred that the position of SPR bands of AuNPs has size-dependency [20]. So the absorption band at the lower wavelength of
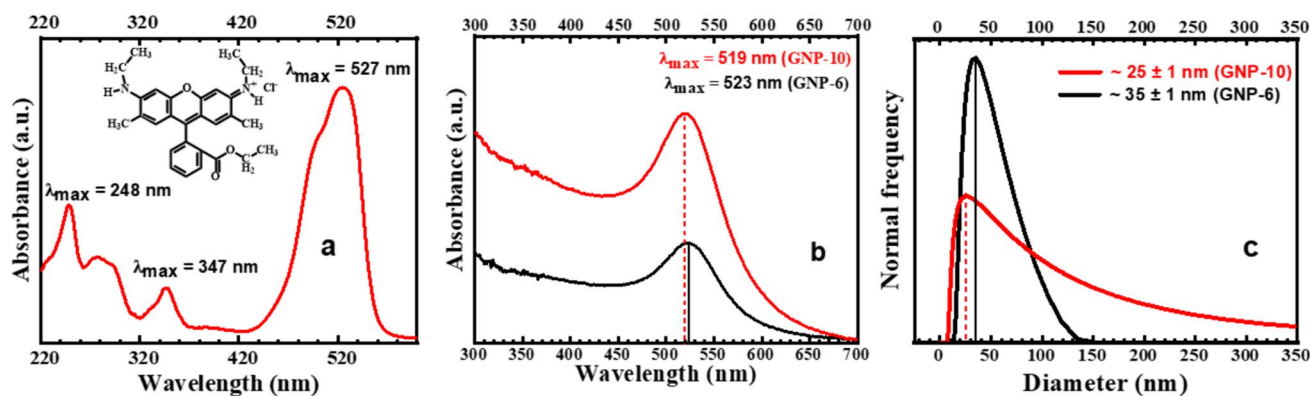
Fig. 1 **a** Absorbance peak of R6G with chemical structure, **b** UV–Vis absorbance spectrum of as-synthesized different AuNPs, and **c** size distribution curve of synthesized AuNPs measured by the DLS method

519 nm indicates the formation of smaller particle sizes, and the electron orbitals move closer to one another, causing the blue shift effect (absorb high energy) and the absorption band at the higher wavelength of 523 nm indicates the formation of large particle sizes due to their overlapping orbitals causing the red-shift effect. These observations of size-dependent AuNPs are further analyzed by DLS and TEM studies and discussed in the following sections.

For proper characterization of synthesized AuNPs, measurement of particle size and surface charge (e.g., Zeta potential) is crucial. From DLS we get the hydrodynamic diameter (particle size) and the Zeta potential value of AuNPs. Figure 1c indicates that our synthesized AuNPs are of ~ 25 ± 1 nm at pH 10.0 (GNP-10) which exhibited Zeta potential of − 17.69 mV and those of AuNPs of size ~ 35 ± 1 nm at pH 6.0 (GNP-6) with Zeta potential of − 32.78 mV. It is observed that the lower SCD concentration leads to larger size AuNPs and higher SCD concentration leads to smaller AuNPs (cf. Figure 1b and c). Therefore, it can be concluded that when the concentration ratio of $HAuCl_4$ and SCD is increased from 2:1 to 1:2, the number of nuclei increases which decreases the AuNPs sizes [21]. Moreover, both the particle size distribution and Zeta potential value increase in acidic conditions. The stability of nanoparticles and their Zeta potentials are related to each other through four potential ranges such as values from − 5 to + 5 mV (aggregation), about ± 20 mV (short time stability), above ± 30 mV (good stability), and ± 60 mV (excellent stability) [22]. Therefore, we can infer that AuNPs of ~ 35 nm (− 32.78 mV) exhibit better stability than those of ~ 25 nm (− 17.69 mV) size. For a more accurate measurement of nanoparticle size as well as direct visualization of their shape, systematic TEM analyses were conducted and discussed in the section below.

Transmission electron microscopy

TEM analyses were performed to estimate the particle size and size distribution directly as well as to verify the shapes and calculate the inter-planer spacing value of the dispersed suspension of AuNPs. As can be seen from Fig. 2a and e, the low-resolution Bright Field (BF) TEM micrographs confirmed that the AuNPs are spherical and almost uniform in size. To get the mean size distributions of AuNPs ImageJ software was used to analyze the TEM images and the average diameter of as-prepared AuNPs was found to be 12 ± 1 nm (GNP-10) and 25 ± 3 nm (GNP-6) respectively (cf. Figure 2b and f). From TEM analysis it is also demonstrated that AuNPs sizes increased with the decrease in the molar ratio of $HAuCl_4$ and SCD. The particle size of the formed AuNPs decreased from ~ 25 nm (GNP-6) to ~ 12 nm (GNP-10) with the increase of the molar ratio of $HAuCl_4$ and SCD from 2:1 to 1:2 [23].

The high-resolution transmission electron microscopy (HR-TEM) images are depicted in Fig. 2c, d, g, and h, where the high crystallinity of the material is indicated by the well-defined lattice fringes. It determines the inter-planar spacing, d_{hkl}, specific to the Miller index (hkl). The estimated d-spacing values of 0.232 nm and 0.222 nm (see Fig. 2c and g) for GNP-10 and GNP-6, respectively, correspond to the d_{111} plane of Au. In contrast, the estimated d-spacing values of 0.209 nm and 0.201 nm (see Fig. 2d and h) for GNP-10 and GNP-6 respectively, correspond to the d_{200} lattice planes of Au [24]. The reduction of the d-spacing value (for the d_{111} plane, the d-value reduced from 0.232 to 0.222 nm, and for the d_{200} plane, the d-value reduced from 0.209 to 0.201 nm) confirmed the size of AuNPs is increased corroborating the literature [25]. It is also confirmed that prepared nanoparticles are AuNPs, and no other impurities are present in the specimen. The particle sizes from DLS and TEM are not well-matched but follow the trend with synthesis conditions
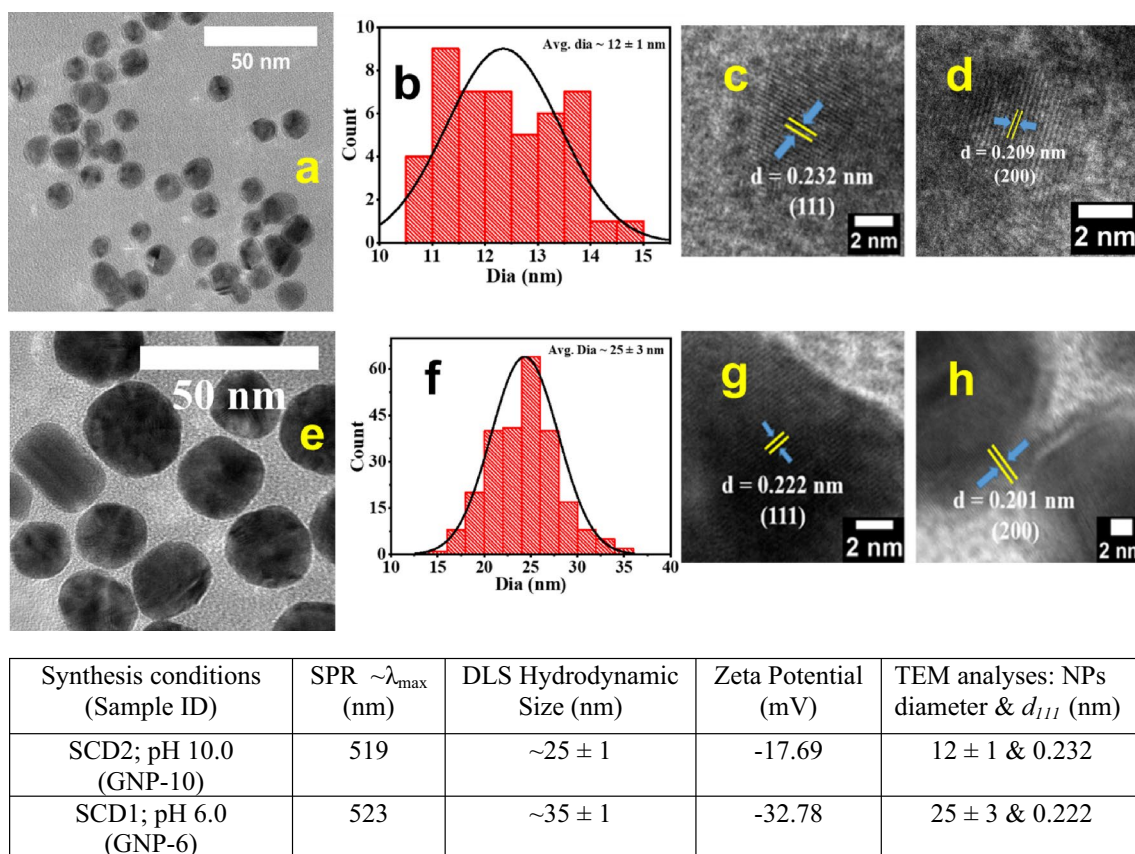
Fig. 2 **a**, **e** TEM Bright Field (BF) images of AuNPs grown at pH 10.0 (GNP-10) and pH 6.0 (GNP-6), **b**, **f** corresponding size distribution; and high-resolution lattice fringe images showing inter-planar spacing (**c**, **g**) correspondent to (111) plane, and **d**, **h** correspondent to (200) plane of AuNPs. The table in the bottom panel summarizes UV–Vis absorption, DLS, and TEM data of spherical AuNPs with their synthesis conditions

Synthesis conditions (Sample ID)	SPR $\sim\lambda_{max}$ (nm)	DLS Hydrodynamic Size (nm)	Zeta Potential (mV)	TEM analyses: NPs diameter & d_{111} (nm)
SCD2; pH 10.0 (GNP-10)	519	$\sim25 \pm 1$	-17.69	12 ± 1 & 0.232
SCD1; pH 6.0 (GNP-6)	523	$\sim35 \pm 1$	-32.78	25 ± 3 & 0.222

(table in Fig. 2). This is because, TEM provides the projected surface area depending on how much incident electrons were transmitted through the specimen, whereas DLS measures the hydrodynamic radius (R_H) of the dispersed particles. Moreover, TEM is a number-based direct measurement technique whereas the DLS is an intensity-based indirect measurement technique ([26] and references therein). As a result, the particle sizes obtained by TEM are usually smaller than those of DLS.

AuNPs size-dependent SERS enhancement

The type of material, size, and shape play the dominant role in determining SERS enhancement. The choice of nanoparticle size for SERS application must be based on experimental data and the comparison between the enhancement effects for a target chemical (SERS probe) when utilizing various nanoparticle sizes [27]. The organic dye, R6G was used to investigate the nanoparticle's size and shape effect on SERS. Figure 3a shows SERS sample preparation on SS substrates (real photographs on the left side, schematic diagram on the
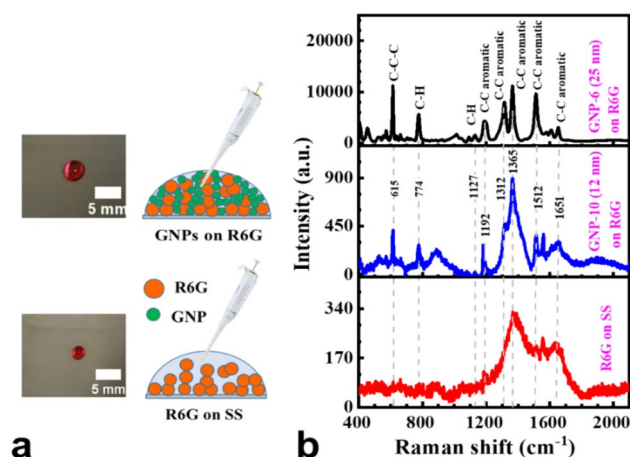

Fig. 3 **a** SERS sample preparation on the stainless steel (SS) base substrate (real photographs on the left side, schematic diagram on the right side), and **b** Raman spectra of R6G (0.2×10^{-3} M) with no, (GNP-10) ~12 nm, and (GNP-6) ~25 nm diameter spherical AuNPs nanoparticles

right side) by using ~ 5 µL of AuNPs solution added in situ atop the 0.2×10^{-3} M R6G droplet (size ~ 4 mm) for Raman spectra recorded for ~ 5 s. The corresponding Raman spectra are displayed in Fig. 3b. As can be seen from Fig. 3b (red curve, bottom panel), R6G without AuNPs addition gives some peaks with a very low intensity. To identify all significant peaks of R6G, prepared GNP-10 and GNP-6 were used and the SERS bands appeared approximately at 615, 774, 1127, 1192, 1312, 1365, 1508, and 1651 cm^{-1}; corroborating the reported bands for R6G molecules [28]. These bands are divided into different groups of vibrational modes, at 615 cm^{-1} for C–C–C ring in-plane, out-of-plane bending for C–H at 774 cm^{-1}, and C–H stretching vibrations at 1127 cm^{-1}, respectively. As well as C–C aromatic stretching vibrations at 1192, 1312, 1365, 1512, and 1651 cm^{-1} [29]. When GNP-6 were given on R6G (Fig. 3b black curve, top panel), the peak position at ~ 615 cm^{-1} shows the highest enhancement of ~ 12,000 counts. In contrast, when GNP-10 were given on R6G (Fig. 3b, blue curve, middle panel) the enhancement is only ~ 450 counts at the same peak position.

When the height of each Raman significant peak of R6G was compared with the SERS peak height of R6G shown in Table S1 [see Supplementary Information (SI) file], GNP-6 on R6G exhibited an average enhancement of ~ 47.49 which is ~ 20 times higher than the enhancement by GNP-10 on R6G. The larger AuNPs of ~ 25 nm (GNP-6) yielded ~ 20-fold larger enhancement factor (EF) than that of ~ 12 nm (GNP-10) AuNPs due to the closeness of the SPR peak of the former to the absorption maxima (λ_{max} ~ 527 nm) of R6G molecules. Moreover, the SERS EF is a crucial parameter for assessing the SERS performance. The SERS EF was calculated by using the equation, $EF = (I_{SERS}/I_{Raman}) \times (C_{Raman}/C_{SERS})$ for considering 615 cm^{-1} band enhancement. For GNP-10 and GNP-6 on R6G, I_{SERS} is ~ 413.41 and ~ 11,235.27 counts, respectively, under constant I_{Raman} (88), C_{Raman} (0.2×10^{-3} M), and C_{SERS} (0.2×10^{-11} M). The calculated EF for GNP-6 on R6G is approximately 2.55×10^{10}, which is significantly higher than that of ~ 9.40×10^{8} for GNP-10 on R6G. The highest EF found in our study is ~ 10^{10}, which corroborates with the theoretical value of the EM enhancement mechanism reported by Le Ru et al. [30]. As a result, ~ 25 nm (GNP-6) sizes of spherical AuNPs were selected for subsequent experiments.

Practical limit of detection (LoD) of R6G

The prepared AuNPs (GNP-6) were used to detect the LoD of R6G in the solution phase. The colour of serially diluted R6G solutions can be seen in Fig. 4a. Figure 4b shows the characteristics of SERS spectra of serially diluted eight different concentrations of R6G solution. For concentrations of 10^{-8}, 10^{-9}, 10^{-10}, and 10^{-11} M a broad hump at 1365 cm^{-1} is
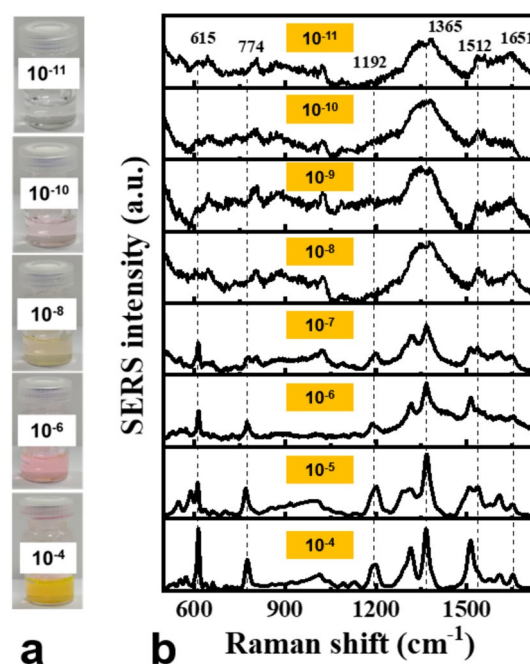

Fig. 4 **a** Dilution of R6G solution with visual colours, and **b** SERS spectra of serially diluted R6G up to 10^{-11} M concentrations

seen instead of a sharp peak. It may be because the number of R6G analyte molecules is decreased with the decrease of its concentration. When the analyte particle is less, the laser is directly imposed on SS and a large hump is observed which is consistent with our previous experiment [17].

Notice that for R6G concentration as low as 10^{-11} M, Raman peaks at 615 cm^{-1}, 1512 cm^{-1}, and 1651 cm^{-1} are still detectable even though with very low intensity. It can be inferred from this study that our SERS protocol can detect R6G at a LoD of 10^{-11} M. In Table S2 (SI file) a comparative study was done for R6G with different SERS substrates and dyes to show the practical utility and effectiveness of our liquid phase SERS protocol for in situ detection of trace level contaminants. Moreover, the advantage of this method is that only 5–10 µL analyte and AuNPs solution without any pre-treatment is enough to take a spectrum within a few seconds.

Conclusion

In this study, we successfully synthesize spherical AuNPs of two different sizes by chemical reduction method utilizing different concentration ratios of HAuCl$_4$ and sodium citrate dihydrate (SCD) showing different pHs of mixture solutions. Both larger and smaller size AuNPs were employed to assess their suitability for the in situ detection of trace contaminants by Surface Enhanced Raman

Spectroscopy (SERS) with R6G as a probe molecule. UV–Vis absorption spectra of as-synthesized AuNPs exhibit surface plasmon resonance (SPR) bands at around 519 and 523 nm and the Dynamic Light Scattering (DLS) technique displayed that the hydrodynamic size (Zeta potential) of $\sim 25 \pm 1$ nm (-17.69 mV) and $\sim 35 \pm 1$ nm (-32.78 mV) for those grown at pH 10.0 (GNP-10) and pH 6.0 (GNP-6), respectively. TEM analysis revealed the average size of spherical nanoparticles to be $\sim 12 \pm 1$ nm (GNP-10) and $\sim 25 \pm 3$ nm (GNP-6) of AuNPs confirming from high-resolution lattice fringes correspond to the d_{111} and d_{200} plane of AuNPs. The ~ 25 nm (GNP-6) Au-NPs on R6G showed that the average enhancement is 47.49 and the highest SERS enhancement factor is $\sim 2.55 \times 10^{10}$. For R6G of 10^{-11} M concentration, four peak positions at 615 cm^{-1}, 774 cm^{-1}, 1365 cm^{-1}, and 1512 cm^{-1} are still observable with very low peak intensity. Our studies demonstrated a simple SERS protocol that could be adopted to detect low-level contaminants in pharmaceuticals, agriculture, and food and foodstuffs in their liquid phase.

Author contributions MSA: Investigation, Data curation, Formal analyses, Writing—original draft; NIT: Methodology, Investigation, Data curation, Formal analysis; MM: Visualization, Resources; MAAS: Visualization, Resources; SFUF: Conceptualization, Methodology, Investigation, Data curation, Formal analyses, Supervision, Funding acquisition, Writing—original draft, Writing—review and editing.

Data availability Data will be made available on reasonable request.

Declarations

Conflict of interest On behalf of all authors, the corresponding author states that there is no conflict of interest.

References

1. A. Nilghaz, S. Mahdi Mousavi, A. Amiri, J. Tian, R. Cao, X. Wang, Surface-enhanced Raman spectroscopy substrates for food safety and quality analysis. J. Agric. Food Chem. **70**(18), 5463–5476 (2022). https://doi.org/10.1021/acs.jafc.2c00089

2. A.K. Malik, C. Blasco, Y. Picó, Liquid chromatography–mass spectrometry in food safety. J. Chromatogr. A. **1217**(25), 4018–4040 (2010). https://doi.org/10.1016/j.chroma.2010.03.015

3. B. Liu, P. Zhou, X. Liu, X. Sun, H. Li, M. Lin, Detection of pesticides in fruits by surface-enhanced Raman spectroscopy coupled with gold nanostructures. Food Bioprocess Technol. **6**(3), 710–718 (2013). https://doi.org/10.1007/s11947-011-0774-5

4. K.M. Abedin, S.F.U. Farhad, M.R. Islam, A.I. Talukder, A.F.M.Y. Haider, Construction and operation of a dispersive laser Raman spectrograph using interference filter. J. Bangladesh Acad. Sci. **32**, 121–129 (2008). https://doi.org/10.3329/jbas.v32i1.2451

5. M.R. Islam, M. Saiduzzaman, S.S. Nishat, A. Kabir, S.F.U. Farhad, Synthesis, characterization and visible light-responsive photocatalysis properties of Ce doped CuO nanoparticles: a combined experimental and DFT + U study. Colloids Surf. A. **617**, 126386 (2021). https://doi.org/10.1016/j.colsurfa.2021.126386

6. S.F.U. Farhad, R.F. Webster, D. Cherns, Electron microscopy and diffraction studies of pulsed laser deposited cuprous oxide thin films grown at low substrate temperatures. Materialia. **3**, 230–238 (2018). https://doi.org/10.1016/j.mtla.2018.08.032

7. K. Dodo, K. Fujita, M. Sodeoka, Raman spectroscopy for chemical biology research. J. Am. Chem. Soc. **144**(43), 19651–19667 (2022). https://doi.org/10.1021/jacs.2c05359

8. S.F.U. Farhad, K.M. Abedin, M.R. Islam, A.I. Talukder, A.F.M.Y. Haider, Determination of ratio of unsaturated to total fatty acids in edible oils by laser Raman spectroscopy. J. Appl. Sci. **9**, 1538–1543 (2009). https://doi.org/10.3923/jas.2009.1538.1543

9. R.G. Nikov, A.S. Nikolov, N.N. Nedyalkov, I.G. Dimitrov, P.A. Atanasov, M.T. Alexandrov, Stability of contamination-free gold and silver nanoparticles produced by nanosecond laser ablation of solid targets in water. Appl. Surf. Sci. **258**, 9318–9322 (2012). https://doi.org/10.1016/j.apsusc.2011.12.040

10. P. Goel, M. Arora, Remediation of wastewater from chlorpyrifos pesticide by nano-gold photocatalyst. MRS Adv. **5**(52–53), 2661–2667 (2020). https://doi.org/10.1557/adv.2020.279

11. F. Tian, F. Bonnier, A. Casey, A.E. Shanahan, H.J. Byrne, Surface enhanced Raman scattering with gold nanoparticles: effect of particle shape. Anal. Methods. **6**(22), 9116–9123 (2014). https://doi.org/10.1039/C4AY02112F

12. F.M. Vieira, C.G. Calisto, C. Izumi, Construction of SERS substrates by gold nanoparticles assembly on polymeric matrices. Appl. Surf. Sci. **612**, 155818 (2023). https://doi.org/10.1016/j.apsusc.2022.155818

13. J. Hu, Z. Wang, J. Li, Gold nanoparticles with special shapes: controlled synthesis, surface-enhanced Raman scattering, and the application in detection. Sensors. **7**(12), 3299–3311 (2007). https://doi.org/10.3390/s7123299

14. S.F.U. Farhad, A.K.M.H. Hoque, N.I. Tanvir, S. Islam, M. Hossain, M.Z. Baten, Enhanced and tunable absorption characteristics of Au-nanoparticle loaded ZnO nanorods grown by hydrothermal technique. In *2021 IEEE International Conference on Telecommunications and Photonics (ICTP)*, 2021, Dhaka, Bangladesh (2021), pp. 1–5. https://doi.org/10.1109/ICTP53732.2021.9744192

15. S.R. Emory, W.E. Haskins, S.M. Nie, Direct observation of size-dependent optical enhancement in single metal nanoparticles. J. Am. Chem. Soc. **120**, 8009–8010 (1998). https://doi.org/10.1021/ja9815677

16. J. Kimling, M. Maier, B. Okenve, V. Kotaidis, H. Ballot, A. Plech, Turkevich method for gold nanoparticle synthesis revisited. J. Phys. Chem. B. **110**(32), 15700–15707 (2006). https://doi.org/10.1021/jp061667w

17. M.S. Alam, S.F.U. Farhad, N.I. Tanvir, M.N.A. Bitu, M. Moniruzzaman, M. Hakim, M.A.A. Shaikh, Spherical and rod-shaped gold nanoparticles for surface enhanced Raman spectroscopy. In: *2022 IEEE 4th International Conference on Sustainable Technologies*

for Industry 4.0 (STI), 2022 (2022), pp. 1–4. https://doi.org/10.1109/STI56238.2022.10103260

18. J.H. Kim, W.W. Bryan, T.R. Lee, Preparation, characterization, and optical properties of gold, silver, and gold–silver alloy nanoshells having silica cores. Langmuir. **24**(29), 11147–11152 (2008). https://doi.org/10.1021/la8016497

19. A.N. Shipway, E. Katz, I. Willner, Nanoparticle arrays on surfaces for electronic, optical, and sensor applications. ChemPhysChem **1**(1), 18–52 (2000). https://doi.org/10.1002/14397641(20000804)1:1%3c18::AID-CPHC18%3e3.0.CO;2-L

20. D.A. Said, A.M. Ali, M.M. Khayyat, M. Boustimi, M. Loulou, R. Seoudi, A study of the influence of plasmonic resonance of gold nanoparticle doped PEDOT:PSS on the performance of organic solar cells based on CuPc/C60. Heliyon **5**(11), e02675 (2019). https://doi.org/10.1016/j.heliyon.2019.e02675

21. X. Ji, X. Song, J. Li, Y. Bai, W. Yang, X. Peng, Size control of gold nanocrystals in citrate reduction: the third role of citrate. J. Am. Chem. Soc. **129**, 13939–13948 (2007). https://doi.org/10.1021/ja074447k

22. S. Honary, F. Zahir, Effect of zeta potential on the properties of nano-drug delivery systems—a review (Part 2). Trop. J. Pharm. Res. **12**(2), 265–273 (2013). https://doi.org/10.4314/tjpr.v12i2.20

23. K. Zabetakis, E.G. William, K. Sanjeev, D. Marie-Christine, Effect of high gold salt concentrations on the size and polydispersity of gold nanoparticles prepared by an extended Turkevich-Frens method. Gold Bull. **45**, 203–211 (2012). https://doi.org/10.1007/s13404-012-0069-2

24. R.T. Mendieta, D. Ventura-Espinosa, S. Sabater, J. Lancis, G. Mínguez-Vega, J.A. Mata, In situ decoration of graphene sheets with gold nanoparticles synthetized by pulsed laser ablation in liquids. Sci. Rep. **6**, 30478 (2016). https://doi.org/10.1038/srep30478

25. K. Okada, T. Nagashima, Y. Kameshima, A. Yasumori, T. Tsukada, Relationship between formation conditions, properties, and crystallite size of boehmite. J. Colloid Interface Sci. **253**(2), 308–314 (2002). https://doi.org/10.1006/jcis.2002.8535

26. S. Bhattacharjee, DLS and zeta potential—what they are and what they are not? J. Control. Release. **235**, 337–351 (2016). https://doi.org/10.1016/j.jconrel.2016.06.017

27. L. Pei, Y. Huang, C. Li, Y. Zhang, B.A. Rasco, K. Lai, Detection of triphenylmethane drugs in fish muscle by surface-enhanced Raman spectroscopy coupled with Au–Ag core–shell nanoparticles. J. Nanomater. **8**, 730915 (2014). https://doi.org/10.1155/2014/730915

28. A. Islam, F. Tasneem, Z.H. Khan, A. Rakib, S.F.U. Farhad, A.I. Talukder, M. Wahadoszamen, Economically reproducible surface-enhanced Raman spectroscopy of different compounds in thin film. J. Bangladesh Acad. Sci. (2021). https://doi.org/10.3329/jbas.v45i1.54255

29. D. Pristinski, S. Tan, M. Erol, H. Du, S. Sukhishvili, In situ SERS study of Rhodamine 6G adsorbed on individually immobilized Ag nanoparticles. J. Raman Spectroscopy. **37**(7), 762–770 (2006). https://doi.org/10.1002/jrs.1496

30. E.C. Le Ru, E. Blackie, M. Meyer, P.G. Etchegoin, Surface enhanced Raman scattering enhancement factors: a comprehensive study. J. Phys. Chem. C. **111**(37), 13794–13803 (2007). https://doi.org/10.1021/jp0687908